Dynamics of shear layers induced by hairpin packets in shallow free-surface flows: implications for gas transfer

David Hurther, Eugene A. Terray, Ulrich Lemmin

Dynamics of shear layers induced by hairpin packets in shallow free surface flows: implication for gas transfer

D.Hurther* & E.Terray

Woods Hole Oceanographic Institution, Woods Hole, U.S.A.

**Current affiliation at Laboratoire des Ecoulements Géophysiques et Industriels, CNRS et INP Grenoble, France*

U.Lemmin

Ecole Polytechnique Fédérale, Lausanne, Switzerland

ABSTRACT: This study addresses the shear-layer organization induced by hairpin packets and the corresponding turbulent kinetic energy (TKE) budget in the outer region of highly turbulent, free-surface shear flows over a fully rough bed. The main emphasis is on the parameterization of the TKE budget in the intermediate and near-surface regions where shear layers dominate production and transport of TKE. We discuss the implications for such processes as gas exchange at the air-water interface, for gas of low solubility. We find that the organization of the outer region proposed by Adrian *et al.* based on hairpin packets agrees well with our open-channel flow data. Using the same conditional sampling method as Adrian *et al.,* we observe similar zones of uniform streamwise momentum. Intense shear layers are seen to extend over the entire outer flow region. The streamwise scale of the hairpin packets correspond well with the longitudinal dimensions found in Adrian *et al.* (typically 1–2 times the boundary layer thickness). Combining an unconventional uw-quadrant threshold technique to instantaneous momentum flux representations, we demonstrate that the shear stress events below a critical threshold are mainly small scale structures that do not contribute to the vertical TKE flux in the outer region. For quasi-instantaneous shear-stress events above the critical threshold, extended homogeneous shear layers are found between the wall region and the free Surface-Influenced Layer (SIL). We find that the TKE flux results from the residual momentum flux between ejections and sweeps above a critical H_{max} value. These data demonstrate the importance of the vertical velocity skewness in the observed shear layer dynamics, in agreement with previous observations by Raupach (1981). Inertial range estimates of TKE dissipation support the idea that dissipation close to the surface is in local balance with TKE transport. Observations indicate that the fraction of surface water renewing eddies is nearly independent of the Reynolds number. This agrees with measurements of boils in the North Sea by Nimmo Smith *et al.* (1999) and with laboratory measurements of upwellings by *Kumar et al.* (1998).

1 INTRODUCTION

Over the past forty years, research on shear turbulence has focused on the dynamics of intermittent quasi-organized flow events, such as streaks, omega and hairpin structures, bursts, vortex heads, ejections, sweeps, boils, upwellings, downwellings, spiral eddies, occurring intermittently at scales that vary with distance from the wall. As pointed out by Robinson (1991) in the review of this topic, most of the studies have been devoted to the flow organization in the inner region $z^+<200$, where z^+ is the normal coordinate normalized by the viscous length. Until the end of the eighties, flow observation capabilities of the measuring tools were limited. The experimental studies resulted in a large number of conceptual models on the bursting phenomenon (Theodorsen 1952, Hinze 1975, Blackwelder and Eckelmann 1979, Bogard and Tiedermann 1986). The concept diversity led to some confusion which has been partially overcome by DNS results. The success of this technique in the study of coherent structures relies on its capability to provide a Lagrangian view of the flow field over arange pf scales extending from the viscous to the integral lengthscales. In turn, important limitations of DNS methods persist in terms of bed-roughness, moderate to high Reynolds

and Froude numbers and stratification effects. These effects appear to be crucial in the study of geophysical shear currents.

Recent studies by Tardu (1995), Zhou *et al.* (1999) Adrian *et al.* (2000) (hereafter referred to as ATM00) significantly contributed to the progress in understanding organized motion in the outer region of flows with high Reynolds number. Their results suggest the existence of hairpin packets in the outer region. A subdivision of the entire boundary layer into three zones is proposed depending on the mean advection velocity spatially-averaged over zones of uniform, retarded streamwise momentum. The major advantage of the hairpin packet model lies in its ability to explain most of the conceptual models of the bursting phenomenon in the inner region as well as the presence of coherent structures in the outer region, the so-called "packets" which scale with outer parameters of the boundary layer. The change of scales with distance from the wall is thereby taken into account. Furthermore, good agreement between numerical (Zhou *et al.* 1999) and experimental results (ATM00) on the hairpin packets organization is found which reinforce the validity of this concept.

In the present work, we check if the hairpin packet concept occurs in the outer region of highly turbulent open-channel flows (Reynolds number with $O(10^4–10^5)$) under fully rough bed situations. Therefore, we aim to determine the sensitivity of this concept to the wall roughness in order to verify whether this concept can or cannot be applied to shear flows under geophysical conditions. Furthermore, we are interested to determine the influence of the free-surface on the hairpin packets organization. Unconventional quadrant threshold techniques are used to investigate these aspects. We will analyze the structure of shear stress and its dependence on the hairpin packets organization. Finally, we will discuss the parameterization of the TKE budget in the intermediate and free Surface Influenced Layer (SIL).

From the previous results, the implications for such processes as the gas exchange at the air-water interface are addressed. A better understanding of turbulence near the free surface is of primary importance for the improvement of gas transfer velocity predictions. We will analyze the effects of the hairpin packets organization on the Turbulent Kinetic Energy (TKE) dissipation rate in the SIL.

We propose a mechanism underlying the gas transfer velocity models considering horizontal inhomogeneities at the free surface. Several studies (Komori *et al.* 1989, Rashidi *et al.* 1991, Nimmo Smith *et al.* 1999) have shown that horizontal inhomogeneities are due to the impinging of large coherent flow structures emanating from the bulk region. As was demonstrated by Moog and Jirka (1999) these models lead to inconsistencies for shear flows with Reynolds above 500 (Reynolds number based on the turbulent macroscale and bed-friction velocity). We will discuss these aspects by revisiting the conceptual model called the "Chain Saw Model" (CSM), derived in Moog and Jirka (1999).

2 EXPERIMENTAL SET-UP

Experiments were carried out in a laboratory open-channel under uniform flow conditions (28m long, 2.4m wide, 1m deep) over a rough bed. A sand bed with a mean grain size of d_{50}=9mm was used. The measurement section is placed 13m downstream from the entrance where the turbulent flow is well developed. All velocity data presented here were taken in the center of the channel. The hydraulic parameters are given in Table 1. These indicate subcritical highly turbulent flow. The standard roughness k_s^+ is normalized with the corresponding viscous lengths and is higher than 70, corresponding to a fully rough bed. The aspect ratio of the flow is larger than 14 ensuring that secondary currents are negligible at the centerline of the flume. The turbulent micro-scale is equal to 1.47cm in the present flow conditions. The spatial resolution of the instrument used herein is less than 4mm which allows to cover the inertial subrange of the turbulent flow.

The 3D Acoustic Doppler Velocity Profiler (3D ADVP) offers the unique possibility of profiling the 3D quasi-instantaneous velocity field simultaneously over the entire boundary layer thickness, corresponding to 99% of the flow depth in uniform open-channel conditions. This instrument is well adapted to the study of turbulent quasi-coherent flow motion in clear-water free-surface flows (Hurther and Lemmin 2000, Blanckeart and DeVriend 2002). Compared to conventional Acoustic Doppler Velocity measurement, we use a correction method to increase the bandwidth of the resolved velocity field (Hurther and Lemmin 2001). TKE budget terms are estimated with an uncertainty below 15%.

3 HAIRPIN PACKETS ORGANIZATION

The occurrence of multiple hairpin structures or clusters of hairpins that form a coherent group or packet, has been anticipated by several pioneering studies on the inner region of zero pressure gradient boundary layers with low Reynolds number (Acarlar and Smith

Table 1. Flow conditions.

Run	δ (cm)	U_∞ (cm/s)	u_* (cm/s)	Re_δ ($\times 10^3$)	Re_θ ($\times 10^3$)	k_s^+	λ (cm)
A	17.2	39.8	2.8	68.45	7.9	280	1.47

1987a and b; Zhou *et al.* 1999). The demonstration of the existence of hairpin packets in the outer region of shear flows at moderate Reynolds number (which is of more interest herein) relies on the unique study by ATM00. This work clearly exhibits the presence of packets composed by several units of hairpin heads arranged along streamwise lines of uniform streamwise momentum. A subdivision of the boundary layer into four zones has been proposed. The first zone is siutated in the inner region, nearly corresponding to the buffer layer where the bursting phenomenon occurs and associated Omega shaped structures emanate. Between this zone and the second one (called Zone I after ATM00's terminology which will be used hereinafter), groups of Omega shaped structures are deformed (vortex stretching occurs under the effect of shear) into packets of hairpins that propagate together with a constant streamwise velocity. Zone I is located at the beginning of the logarithmic layer and therefore is part of the outer region. At this stage, the size of the packets is relatively small compared to the size of the packets in Zones II and III. Zone II which is still located in the logarithmic layer is characterized by packets of hairpins that are well delimited by domains of uniformly retarded fluid. The typical size of the packets in this zone is 1.2δ (where δ corresponds to the boundary layer thickness). The characteristic growth angle of the packet is found to be smaller than the growth angle of the individual hairpin structures in a packet. It has been shown that the growth angle of the individual hairpins in the packets appears to increase with distance from the wall. Close to the head the individual hairpin inclination varies between 45° and 90°. The inclination of the packet, however, is found to remain linear quite frequently over the three zones. The mean angle varies between 3° and 35° with a mean value of around 10°. In Zone III, the packets are less retarded compared to the packets of Zone II. They represent older packets that have been generated upstream by packets of Zone II.

The characteristic features found by ATM00 in Zones I to III are observed in Figure 1. It shows the data taken at the centerline of the open-channel flow. The grey zones represent regions of uniform streamwise

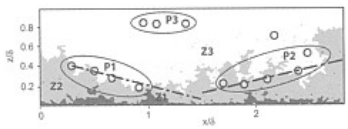

Figure 1. Hairpin packets and subdivision into zones of uniform streamwise momentum of the outer region of open-channel flow Histogram.

velocity defined as $u-U_d/u_*$. u is the instantaneous streamwise velocity component. U_d is the depth averaged velocity. Three ranges of levels are represented. The dark gray range corresponds to values lower than −2.5, the lighter grey region ranges from −2.5 to −1.8 and the white levels corresponds to values higher than −1.8. The three zones show the presence of regions of uniform streamwise momentum that are very similar to the zones observed in ATM00. The ranges of the values corresponding to the different zones also agree to the values found by ATM00 for their high Reynolds number experiment. As shown in Table 1, the Reynolds numbers of both experiments are very similar. Furthermore, the circles in Figure 1 denote regions of high transverse vorticity supposed to correspond to the heads of hairpin structure in the outer region. Three packets called P1, P2 and P3 are observed over a streamwise distance of 3δ. Here δ, the boundary layer thickness, corresponds to 99% of the flow depth. A very robust criteria of similarity between ATM00 observations and our data is observed in the location of the hairpin heads of P1 and P2 on the separation line between Zone II and Zone III. The size of the packets in Zone II again matches well with the size indicated in ATM00 (roughly equal to δ). The approximation of the growth angle of P2 is given by the inclination of the dashed dotted line. We find a value of 18° which lies in the range found in ATM00. The inclination of P1 is seen to be negative. However, this occurs rarely in our data.

Overall we deduce that we find good agreement between the zone subdivision in the open-channel flow and in the free-stream boundary layer of ATM00. Nevertheless, it seems that the lines of separation between the different zones are smoother in AMT00's results. Since these discrepancies can not be attributed to Reynolds numbers differences between the two experiments (considering the high Reynolds experiment in AMT00), we suspect bed roughness effects.

The previous discussion was based on qualitative aspects. A more quantitative proof that the hairpin organized motions in the outer region are induced in three zones of uniform streamwise momentum can be attempted by evaluating the probability density function (PDF) of the instantaneous longitudinal velocity. As discussed in ATM00, the size of the data sample should be small, roughly equal to the mean length of hairpin packets, i.e. around δ. Such a PDF is shown in Figure 2. The averaging can be interpreted as a spatial average over the entire boundary layer thickness and over a time period roughly corresponding to $t=\delta/U_d$. As can be seen, three local maxima (U_{z1}/U_∞=0.45, U_{z2}/U_∞=0.79, U_{z3}/U_∞=0.97, U_∞ is the time averaged velocity at 99% of the flow depth) can be distinguished. They correspond to the first order moment of three approximated probability density subfunctions. ATM00 have found very similar PDF

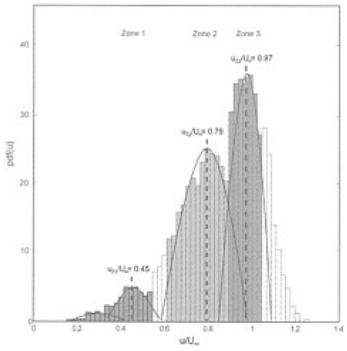

Figure 2. Histogram of the relative instantaneous velocity component u.

and corresponding modal velocities, U_{z1}/U_∞=0.59, U_{z2}/U_∞=0.76, U_{z3}/U_∞=0.94, for the high Reynolds number flow.

From the good agreement between ATM00's data and the present open-channel flow data we conclude that hairpin packet organized motion is also found in open-channel flows over completely rough beds. At this stage we cannot distinguish any effects of the free-surface on the turbulent motion of the outer region.

4 STRUCTURE OF SHEAR STRESS IN THE OUTER REGION

The quadrant threshold technique proposed by Lu and Willmarth (1973) has been used originally to study the bursting phenomenon in the buffer region of shear flows. Since then, many studies (Bogard and Tiederman 1987, Sechet and Leguennec 1999) have applied this technique to point measurements throughout the entire boundary layer. The ability of the 3D ADVP to profile quasi-instantaneously over the entire boundary layer, offers a greatly extended possibility to study organized flow motion.

The quadrant threshold technique, which provides quantitative information on the momentum flux structure, can be used in visualizing instantaneous flow field features (Figure 3). Figure 3a shows the effect of the conditional sampling on the relative amplitude of $u'w'(z, t)$ in the (u', w') plane at a given depth z. The thin and thick hyperbolic curves correspond to the functions $u'w'/\overline{u'w'} < |H|$ are called the

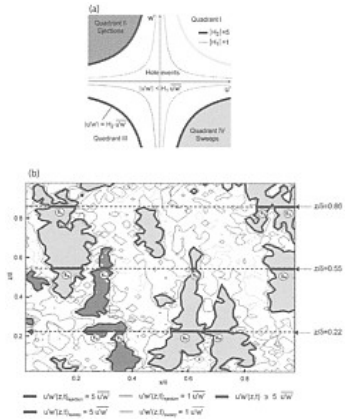

Figure 3. The quadrant threshold technique and its effects on the instantaneous flow velocity field. (a) Representation of constant isolines of relative momentum flux $u'w'$ in the (u', w') plane. (b) Representation of conditionally sampled momentum flux for low and high threshold values, respectively for H=1 (thin lines) and H=5 (thick lines).

hole-events. Figure 3b shows the effect of the threshold selection on the instantaneous momentum flux field. The flow patterns delimited by the thin and thick lines again correspond to the regions $u'w'/\overline{u'w'} \geq |H|$ for H equal to 1 and 5 respectively.

In Figure 3b, the thick and thin lines represent isolines of high and low relative momentum flux, respectively. As suggested by the results in Figure 3b, only ejections and sweeps contribute significantly to the total shear stress $\overline{u'w'}$ for H=5. Outward and inward interactions events can not be distinguished in this figure. Furthermore, several high shear stress patterns in Zone III are not attached to the wall layer which suggests that they might not be a direct consequence of the bursting phenomenon occurring in the wall layer. Instead they may depend on a large scale hairpin organization of the outer region. It is also seen that for larger H values the small-scale shear stress structures (ejections and sweeps) are not selected and are generally detached from the high shear structures with much larger spatial scales. This aspect is clearly indicated by the important number of small-scale structures delimited by the thin lines and the very few small-scale structures delimited by the thick lines in Figure 3b (except at coordinates (0.6, 0.95) and (0, 0.22)). The patterns in Figure 3b show elongated

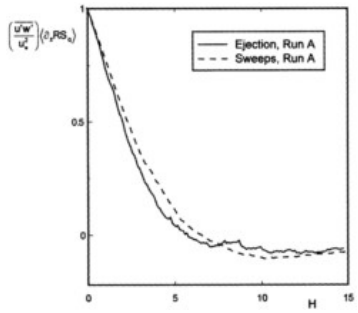

Figure 4. Vertical gradient of momentum flux $u'w'$ corresponding to ejection and sweeps as a function of H. The brackets denote a spatial average over the domain $0.2<z/\delta<0.7$.

shear layers which are composed of an extended core region surrounded by smaller scale shear stress structures corresponding to structures with lower H value. One may speculate from these observations that the frontiers of the large coherent shear layers interact with the surrounding less coherent fluid because of their relatively low momentum flux. The latter are probably more isotropic structures since they are not detected by the quadrant threshold technique. The interaction seems to occur at much lower scales than the mean scale of the core region corresponding to high H values.

In order to quantitatively verify the existence of high shear stress events with a uniform core region, Figure 4 represents the vertical gradient of the momentum flux of ejections and sweeps as a function of the threshold H. In this figure, the momentum flux is normalized by the squared bed friction velocity rather than by the mean local shear stress value. The brackets < > denote that the quantity has been spatially averaged over the region $0.2\leq z/\delta\leq 0.75$. It can be seen that ejections and sweeps reach a negligible vertical gradient for $8\leq H\leq 9$. The average value of the vertical gradient is equal to 5.9 and is taken at 10% of its maximum. This result strongly supports the existence of elongated shear layers with a uniform vertical core region in Zones II and III.

The combination of an unconventional quadrant technique with instantaneous flow field observations has provided insight into the dynamical details of the shear layers that exhibit a core region of uniform shear in the vertical direction. The vertical size of the shear layers is observed to scale with the vertical dimensions of Zones II and III corresponding to outer flow length scales. The uniform core regions of the shear structures are typically delimited by isocontours of values equal to 5 or above. The shear layers are found to be surrounded by smaller scale shear stress structures selected by threshold values typically lower than 2. This observation suggests that these events are related to the large-scale organization of the outer region (hairpin packets) and depend weakly on the internal small-scale organization of the wall layer. Their uniformity also implies that they weakly depend on the internal structures of the hairpin packets.

5 TKE BUDGET IN THE OUTER REGION: THE ROLE OF ELONGATED SHEAR LAYERS

Figure 5 shows the profile of the normalized difference between the shear production and the TKE dissipation rate (dashed line). The profile of the normalized TKE transport term (solid line) is also presented in Figure 5. The TKE dissipation is compensating the TKE transport in the near surface region. The shear production is negligible in this region because the vertical gradient of mean longitudinal velocity is negligible. From this observation we also infer that the SIL can be defined as the region corresponding to $z/\delta\geq 0.7$. The value of the normalized dissipation very close to the free surface tends towards unity. This agrees well with the measurements by Nezu and Nakagawa (1993). In order to investigate the dynamical details of this balance in the outer region, we present the profile of the normalized vertical TKE flux (called F_k) in Figure 6. A region of constant F_k is observed over an extended region corresponding to $0.15\leq z/\delta\leq 0.7$. As discussed by Lopez and Garcia (1999) and Hurther and Lemmin (2000), this region reveals the presence of a dynamical equilibrium between production and dissipation in the outer region. In the SIL, the equilibrium is found to be affected by the free surface for $z/\delta\geq 0.7$. The constant slope of the F_k curve in the layer explains the nearly constant TKE dissipation profile shown in Figure 5.

We intent to determine to what extend the shear layers detected by the quadrant threshold technique for high H values contribute to F_k in the outer region. As can be deduced from the literature results on the quadrant contribution (Nakagawa and Nezu 1977, Raupach 1981, Hurther and Lemmin 2000), it is not likely that the sum of ejections and sweeps contributes to F_k since they are mainly responsible for the shear production. Raupach (1981) has pointed out, however, that the difference between the contribution of ejections and sweeps can be strongly correlated to F_k in the outer region. The following expression has been proposed:

$$F_k = 0.75\,\Delta S\left(c_1\sigma_w^2\sigma_w + c_2\sigma_w^3\right) \tag{1}$$

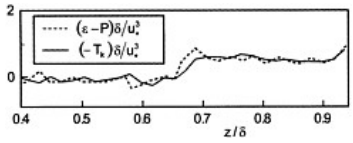

Figure 5. Profile of the difference between normalized shear production and TKE dissipation rate and profile of the TKE transport term.

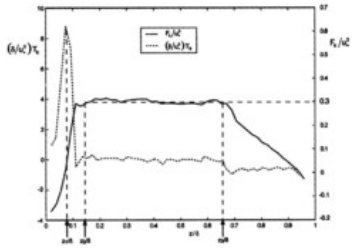

Figure 6. Profile of the normalized TKE flux F_k and the vertical TKE transport term T_k.

ΔS is equal to the difference between the relative shear stress (relative to the local mean value) due to ejection and sweep events for H=0. Eq.(1) is a semi-theoretical derivation of F_k because it relies on the experimental evidence that the third order moments (skewness, kurtosis, crossed-third order moments) are found to be linearly related over the outer region of the turbulent boundary layer (Raupach 1981, Hurther and Lemmin 2003).

Our motivation to analyze the dynamical details of the relation between F_k and ΔS relates the following

– ΔS is found to be positive in the outer region (Nakagawa and Nezu 1977, Raupach 1981, Hurther and Lemmin 2000) which results in an ascendant momentum flux. The TKE flux F_k is also ascendant in the outer region (see Figure 6).

– The depth where F_k changes its sign coincides very well with the depth where the sign of ΔS changes (see Hurther and Lemmin 2000).

– For H>6, corresponding to the value for which the vertical gradients of ejections and sweeps are negligible, the difference between ejections and sweeps, i.e. the ΔS for values of H>6, is uniform over a region roughly corresponding to 0.2<z/δ<0.75 (Figure 4). As can be seen in Figure 6, this region coincides with the region where F_k is constant.

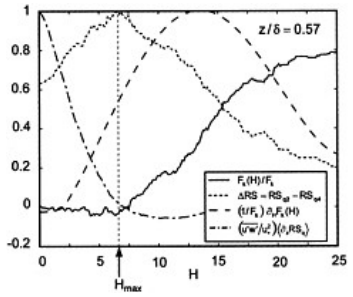

Figure 7. Conditionally sampled AS (dotted line), F_k (solid line) and curve in Figure 4 (dashed dotted line, see Figure 4 for details). The dashed line represents the relative derivative in H of the conditionally sampled Fk curve.

Based on these arguments, we suggest that the residual ascendant momentum flux resulting from the elongated shear layers detected with the quadrant technique for H values roughly above 5, (discussed in Section 4, Figure 3) could be responsible for the TKE flux shown in Figure 6.

To verify this hypothesis on a more quantitative basis, we compare the curve of ΔS as a function of H to the curve of F_k conditionally sampled as a function of H. Note that as H increases, ΔS is equal to the difference between mean ejection and sweep contributions for $u'w'(t, z/\delta) \le H\ \overline{u'w'}$ do not contribute to F_k. Furthermore; it is seen that F_k varies from 0 to 1 as H increases. This shows that the shear stress is the leading turbulent stress in the generation of F_k in the outer region. Normal stresses seem to provide a weak contribution.

Finally, we also observe in Figure 7 that the H value for which the elongated shear stress events have a uniform vertical region agrees very well to H_{max}. The dashed dotted curve in Figure 7 has been redrawn from Figure 4.

We find very similar trends for the curves in the region $0.2 \leq z/\delta \leq 0.7$ (not shown here). This region corresponds well to the region of constant F_k (see Figure 6). Above and below this domain, the ΔS curve is very weakly correlated to the F_k curve (not shown here).

6 IMPLICATIONS FOR GAS TRANSFER AND CONCLUSIONS

As discussed in section 5, we suggest that the elongated shear stress layers associated to the hairpin organization of the outer flow region are responsible for the TKE dissipation rate in the SIL. The TKE implied in this transport results from a residual ascendant momentum flux induced by the asymmetrical contribution to shear stress from ejections and sweeps. As a consequence, small scale turbulence in the outer region makes a very negligible contribution to F_k in the region $0.2 \leq z/\delta \leq 0.7$. In the SIL, however, the TKE diffused through the equilibrium region is dissipated into heat, evidently dominated by small scale isotropic eddies.

This concept is very different from the commonly accepted concept which explains the values of TKE dissipation close to the free surface. Generally it is assumed that the residue of TKE resulting from the difference between shear production and dissipation in the inner region is transported by turbulent diffusion towards the free surface where it interacts. It appears from our results that the vertical transport of TKE mostly depends on the organization of the large turbulent flow structures in the outer region. In this region hairpin packets and associated elongated shear layers dominate the TKE transport between the bottom and the top of the boundary layer.

This result has important implications for the prediction of gas transfer velocities in shear flows. Moog and Jirka (1999) have discussed the validity of the different approaches. They distinguished between two categories of models for the gas transfer velocity estimation. The first one considers the renewal of the water in the CBL (Concentration Boundary Layer of size O(10μm)) through the action of turbulent micro structures that scale with the Kolmogorov scale. The second category considers the characteristics of intermittent coherent flow structures impinging on the free surface (Komori *et al.* 1989, Rashidi *et al.* 1991). Their detailed analysis revealed that models with burst characteristics are unreliable for shear flows with $Re_* \geq 400$. The small-scale models on the other hand, give good results for highly turbulent flows. As pointed

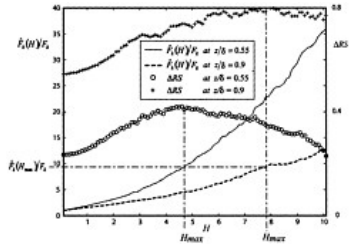

Figure 8. Determination of $\hat{F}_k(H_{max})$ from the conditionally sampled ΔS (dotted line) and F_k (solid line) at z/δ=0.55 and z/δ=0.9.

out in their study, these models "do not provide a comprehensive depiction of turbulence interactions with the free-surface".

To advance the understanding, Moog and Jirka (1999) proposed a conceptual mechanism that includes the non-homogeneity of turbulence at the free-surface due to coherent flow structures: the so-called "Chain Saw Model" (CSM). In this model, the TKE dissipation ε is written as follows:

$$\varepsilon = \left(A_p^+\right)\varepsilon_p \tag{2}$$

A_p^+ must be independent of Re_* for $Re_* \geq 400$, for the model results to match the small scale model results. From the previous results on the shear layer dynamics we propose to evaluate this quantity indirectly as:

$$A_p^+ = 1 - \hat{F}_k(H_{max})/F_k \tag{3}$$

where $A_p^+ \cong 0.8$ in a flow where $Re_* = O(10^6)$. In another open-channel flow experiment, Kumar *et al.* (1998) have estimated the area of the active gas tranfer zone (patterns of large surface divergence at the free-surface). From their surface fraction measurement, the mean surface fraction is close to 0.8. This result agrees as well with our estimation. In their experiments, Re_* is

equal to 411 whereas Re_* is equal to 6800 in our flow. The good agreement found between the three A_P^+ is independent of Re_* as proposed by Moog and Jirka (1999).

Further investigations are conducted to validate this result by direct measurement of the surface fraction of shear layers impinging at the free-surface and its relation to the hairpin packets organization in the outer region. This mechanism is of primary importance for free-surface processes in geophysical shear currents.

ACKNOWLEDGEMENTS

The first author expresses his gratitude to the Post-doctoral Scholar Program at the Woods Hole Oceanographic Institution, with funding provided by the J. Seward Johnson Fund/Allyn Vine Senior Technical Staff Award. This is a Woods Hole Oceanographic Institution contribution No. 10911.

REFERENCES

Acarlar, M.S. Smith, C.R. 1987a. A study of hairpin vortices in a laminar boundary layer. Part 1. Hairpin vortices generated by a hemisphere protuberance. J. Fluid Mech. 175, 1–41.

Acarlar, M.S. Smith, C.R. 1987b. A study of hairpin vortices in a laminar boundary layer. Part 1. Hairpin vortices generated by fluid injection. J. Fluid Mech. 175, 43–83.

Adrian, R.J. Meinhart, C.D. Tomkins, C.D. Vortex organization in the outer region of the turbulent boundary layer. J. Fluid Mech. 422, 1–54.

Blackwelder, R.F. Eckelmann, H. 1979. Streamwise vortices associated with the bursting phenomenon. J. Fluid Mech., 94:577:594.

Blanckeart, K. DeVriend, H. (2002) Turbulence structure in an open-channel bend. Submitted for publication.

Bogard, D.G. Tiedermann, W.G. 1986. Burst detection with single-point velocity measurements. J. Fluid Mech., 162, 389–413.

Bogard, D.G. Tiedermann, W.G. 1987. Characteristics of ejections in turbulent channel flow J. Fluid Mech., 179, 1–79.

Hinze, J.O. 1975. Turbulence. McGraw-Hill, 790 pp.

Hurther, D. Lemmin, U. 2000. Shear stress statistics and wall similarity analysis in turbulent boundary layers using a high resolution 3-D ADVP. IEEE Ocean engineering. 25, 446–457.

Hurther, D. Lemmin, U. 2001, A correction method of mean turbulence measurements with a 3-D acoustic Doppler velocity profile. J. Atm. and Ocean. Tech. 18, 446–458.

Hurther, D. Lemmin, U. 2003. Momentum flux and particle flux statistics in suspension flows. Water Resources Research (accepted for publication).

Komori, S. Murakami, R. Ueda, H. 1989, The relationship between surface-renewal and bursting motions in an open-channel flow. J. Fluid Mech. 203, 103–123.

Kumar, S. Gupta, R. Banerjee, S. 1998. An experimental investigation of the characteristics of the free surface turbulence in open channel flows. Phys. Fluids 10, 437–456.

Lu, S.S. Willmarth, W.W. 1973. Measurements of the structure of the Reynolds stess in a turbulent boundary layer. J. Fluid Mech., 60, 481–511.

Lopez, F. Garcia, M. 1999. Wall similarity in turbulent open channel flow. J. of Eng. Mech. 125, 789–796.

Nakagawa, H. Nezu, I. 1977. Prediction of the contribution to the Reynolds stress from bursting events in open-channel flows. J. Fluid Mech. 80, 99–128.

Nezu, I. Nakagawa, H. 1993. Turbulence in open-channel flows. AIHR Monograph series. Balkema, 281 pp.

Nimmo Smith, W.A.M. Thorpe, S.A. Graham, A. 1999 Surface effects of bottom-generated turbulence in a shallow tidal sea. Nature, 400, 251–253.

Moog, D.B. Jirka, G.H. 1999 Air-water gas transfer in uniform channel flow. ASCE J. Hydraulic Engineering 125, 3–10.

Rashidi, M. Hetsroni, G. Banerjee, S. 1991. Mechanisms of heat and mass transport at gas-liquid interfaces. Int J. Heat Mass Transfer, 34(7), 1799–1810.

Raupach, M.R. 1981. Conditional statistics of Reynolds stress in rough wall and smooth wall turbulent boundary layers. J Fluid Mech., 108, 363–382.

Robinson, S.K. 1991. Coherent motions in the turbulent boundary layer, Annu. Rev. Fluid Mech. 23, 601–639.

Séchet, P. LeGuennec, B. 1999 Near wall turbulent structures and bedload transport. J of Hydr. Res.

Tardu, F.S. 1995. Characteristics of single and clusters of bursting events in the inner layer. Exp. in Fluids, 30, 112–124.

Theodorsen, T. 1952. Mechanism of turbulence, Proc. Mid-west Conf. Fluid Mech., 2nd, Columbus, Ohio, pp. 1–18.

Zhou, J. Adrian, R.J. Balachandar, S. and Kendall, T.M. 2000, Mechanisms for generating coherent packets of hairpin vortices in channel flow. J. Fluid Mech. 387, 353–396.